PAPER • OPEN ACCESS

Semiclassical dynamics of a rigid rotor: SO(3) covariant approach

New Journal of Physics
The open access journal at the forefront of physics

Deutsche Physikalische Gesellschaft DPG
IOP Institute of Physics

Published in partnership with: Deutsche Physikalische Gesellschaft and the Institute of Physics

OPEN ACCESS

RECEIVED
12 November 2014

REVISED
2 March 2015

ACCEPTED FOR PUBLICATION
5 March 2015

PUBLISHED
13 April 2015

PAPER

Semiclassical dynamics of a rigid rotor: SO(3) covariant approach

J L Romero[1], **A B Klimov**[1] **and S Wallentowitz**[2]

[1] Departamento de Física, Universidad de Guadalajara, Revolución 1500, 44410 Guadalajara, Jalisco, Mexico
[2] Instituto de Física, Pontificia Universidad Católica de Chile, Casilla 306, Santiago 22, Chile

E-mail: klimov.andrei@gmail.com

Keywords: phase-space, rigid rotor, semiclassical

Abstract

A semi-classical analysis of the quantum rigid-rotor motion based on a phase-space description of the rotation in terms of a SO(3) covariant Wigner-like distribution is presented. The results are applied to the description of the intense-field alignment of an anisotropically polarizable molecule with high rotational excitation.

1. Introduction

The visualization of quantum systems in phase space is a useful tool for the 'identification' of states by invoking our classical intuition about the shape of statistical distributions and the interference patterns between them [1–3]. The main idea of this approach consists in mapping quantum states on distributions (symbols) on some classical phase space. The self-dual symbols, which arise when the same type of mapping is used both for the density operator and for the observables in order to compute average values by convoluting corresponding symbols, are usually called Wigner symbols[3]. The properties of such mappings essentially depend on the symmetry of the quantum system and on the requirements of covariance under a certain group of transformations [4–14]. In the simplest case of harmonic oscillators and spin-like systems, the transformation groups—Heisenberg–Weyl and SU(2), respectively—are easily identified. The corresponding phase spaces can be constructed in a standard way if the operators from the group representation act irreducibly in the Hilbert space of the quantum system. In the simplest example of spin-like systems this corresponds to subspaces with a fixed value of the spin or orbital quantum number. The situation is more involved when a quantum system with natural action of some dynamic group belongs simultaneously to several invariant (under the group action) subspaces or may 'transit' between irreducible subspaces in its course of evolution. This is precisely the situation of a quantum rotor, with its natural transformation group being SO(3), when the total angular momentum is changed due to the action of an external agent. The concept of a phase-space for such a system can be obtained, adopting different points of view and demanding different types of covariance of the mappings from operators to c-number distributions [15, 16]. The advantage of using one or another mapping depends crucially on the class of states and limiting cases that are of physical interest.

It is worth noting that in the framework of a phase-space approach one not only can visualize states of quantum systems but also may develop specific perturbation theories in the semiclassical limit. This can be achieved by expanding the image of the Heisenberg equation for the density operator, the so-called Moyal equation [17], in a series with respect to a small (semiclassical) parameter. Neglecting higher-order derivatives, one arrives then at a first-order Liouville-type equation [18] that describes the time evolution of the initial phase-space distribution via trajectories defined by a set of first-order ordinary differential equations. The choice of the mapping is particularly important in the semiclassical limit, when the 'physical' parameter is the number of total excitations of the quantum system. Then, an adequate choice of covariance requirements leads to the classical Hamiltonian equations in terms of standard physical observables and the dynamics of quantum systems, with large numbers of excitations that can be successfully analyzed in terms of a phase-space description for sufficiently long times [19–24].

[3] Although non-self-dual mappings are also frequently used, especially for representation purposes.

In this paper we provide a semiclassical analysis of the quantum rigid-rotor motion that is based on a phase-space description of the rotation, using a Wigner-like mapping with SO(3) symmetry. The SO(3) covariant mapping allows us to semiclassically expand the phase-space distribution and the equation of motion based on the physically meaningful parameter of rotational energy. In this way we arrive at the standard Hamiltonian equation describing the rigid-rotor motion. In particular, we show how classical trajectories in phase space emerge and how such a set of trajectories generates the time-dependent phase-space distribution of the rigid rotor. Each trajectory lives in a four-dimensional space, and thus only four coupled equations of motion have to be solved. Expectation values can be obtained as statistical averages over the initial distribution from which the semiclassical trajectories originate. In particular, we apply our treatment to the description of the intense-field alignment of anisotropically polarizable molecules with high rotational excitations and study the degree of alignment.

The paper is organized as follows: in section 2 the SO(3) covariant mapping and the resulting generalized Wigner function are introduced. A more intuitive classical phase-space picture is then elaborated in section 3 by applying a suitable rotation of the reference system. In section 4 we apply our results to a rigid rotor in an external field that tends to align the rotor's axis. The numerical solution to this problem is then shown in section 5. Finally a summary and conclusions are given in section 6.

2. Generalized SO(3) Wigner function

In this section we briefly outline a generalized Wigner-like mapping for systems with SO(3) symmetry that maps Hilbert space to a meta-phase space introduced in [25] (for the covering SU(2) group). The latter is parametrized by three Euler angles $\Theta = (\phi, \theta, \psi)$ adapted to the rotor description, i.e., considering only integer values of the angular momentum. The ranges of values for these angles are therefore $\phi \in [0, 2\pi)$, $\theta \in [0, \pi]$, and $\psi \in [0, 2\pi)$.

The mapping is defined as

$$\hat{f} \Leftrightarrow \left\{ W_f^j(\Theta),\, j = 0,\, 1,\, \ldots \right\}, \tag{1}$$

where the j-symbol of an operator $\hat{f}$ is obtained by tracing it over a kernel,

$$W_f^j(\Theta) = \mathrm{Tr}\left(\hat{f}\, \hat{\omega}_j(\Theta) \right), \tag{2}$$

with the kernel being defined as

$$\hat{\omega}_j(\Theta) = \hat{D}(\Theta)\, \hat{\omega}_j(0)\, \hat{D}^\dagger(\Theta), \tag{3}$$

$$\hat{\omega}_j(0) = \sum_{K=0}^{j} \sum_{q=-K}^{K} \sqrt{\frac{2K+1}{j+1}}\, \hat{T}_{Kq}^{\frac{j+q}{2}\,\frac{j-q}{2}}. \tag{4}$$

Here the rotation operator is given as

$$\hat{D}(\Theta) = \mathrm{e}^{-\mathrm{i}\phi \hat{L}_z}\, \mathrm{e}^{-\mathrm{i}\theta \hat{L}_y}\, \mathrm{e}^{-\mathrm{i}\psi \hat{L}_z}, \tag{5}$$

and the irreducible tensor operator reads

$$\hat{T}_{Kq}^{j'j} = \sum_{mm'} \sqrt{\frac{2K+1}{2j'+1}}\, C_{jm\,Kq}^{j'm'} \left| j',\, m' \right\rangle \langle j,\, m| \tag{6}$$

where $C_{jm\,Kq}^{j'm'}$ are the Clebsch–Gordan coefficients.

The reconstruction relation for the j-component (equation (8)) of the operator is

$$\hat{f}_j = \frac{j+1}{8\pi^2} \int \mathrm{d}\Theta\, W_f^j(\Theta)\, \hat{\omega}_j(\Theta), \tag{7}$$

where $\mathrm{d}\Theta = \sin\theta \mathrm{d}\theta \mathrm{d}\phi \mathrm{d}\psi$ and the completely reconstructed operator is then obtained as

$$\hat{f} = \sum_j \hat{f}_j. \tag{8}$$

This allows us to express a trace over a product of two operators as an overlap integral of their j-symbols:

$$\mathrm{Tr}\left(\hat{f}\hat{g} \right) = \sum_j \frac{j+1}{8\pi^2} \int \mathrm{d}\Theta\, W_f^j(\Theta)\, W_g^j(\Theta). \tag{9}$$

This mapping is covariant under transformations from the SO(3) group and permits us to represent the complete operator in terms of c-valued functions and not only its components in each SO(3) irreducible subspace. As we will see below, the covariance of the map (equations (1)–(4)), results in the possibility to introduce a natural semiclassical parameter inversely proportional to the index j, i.e., related to the rotor angular momentum.

The particular case when $\hat{f}$ acts in a single SO(3) invariant subspace corresponds to $q = 0$ in equation (4), from which the standard Stratonovich–Weyl symbol (independent of the angle ψ) in the irreducible subspace of dimension $j + 1$ [12–14] is reconstructed.

As an example, the j-symbol of the total angular momentum operator $\hat{J}^2$ results as

$$W^j_{J^2}(\Theta) = \frac{j}{2}\left(\frac{j}{2} + 1\right) \sum_{n=0,1,\ldots} \delta_{j,n}, \tag{10}$$

which is obviously a constant in each irreducible subspace.

For the operator $\hat{n}_z = \widehat{\cos\theta}$, for example, that can be written as

$$\hat{n}_z = \int \mathrm{d}\Omega \cos\theta \, |\theta, \phi\rangle\langle\theta, \phi|, \tag{11}$$

with $\mathrm{d}\Omega = \sin\theta \mathrm{d}\theta\mathrm{d}\phi$ (here θ and ϕ denote angles in the configuration space) and

$$|\theta, \phi\rangle = \sum_{l,m} Y^*_{lm}(\theta, \phi)\,|l, m\rangle. \tag{12}$$

The j-symbol has a non-trivial form and depends on the angle ψ:

$$W^j_{n_z}(\Theta) = \sin\theta \cos\psi \sum_{n=0,1,..} \delta_{j,2n+1}. \tag{13}$$

This operator mixes different SO(3) irreducible subspaces. One can observe that only odd values of j are admissible in this case.

The exact image of the von Neumann equation for the density operator is quite involved and can be obtained from the explicit form of the star product [25]. In the semiclassical limit, i.e., for the initial states distributed among SO(3) irreducible subspaces of large dimensions, $j \gg 1$, and localized in the angles Θ in each j-subspace (i.e., the relative fluctuations of the angles θ and ϕ is $\lesssim j^{-1/2}$, respectively), one arrives at the truncated evolution equation for the Wigner function W^j_ρ, being the j-symbol of the density matrix (equation (2)). It has the form of Poisson brackets on a four-dimensional manifold, where the index j is considered as a dynamical variable, $W^j_\rho(\Theta) \approx W_\rho(\Theta, j)$, so that

$$\partial_t W_\rho = 2\left\{W^j_H, W_\rho\right\} + O\left(j^{-2}\right), \tag{14}$$

where W^j_H is the j-symbol of the Hamilton operator. In this case the Darboux coordinates are $((j + 1)\cos\theta, \phi)$ and (j, ψ) (so that the Poisson bracket operator is of order j^{-1}). This has a clear physical meaning: the projection $(j + 1)\cos\theta$ of the momentum j to the fixed axis z generates ϕ-rotations in the laboratory reference frame, while the momentum j produces ψ-rotations in the moving frame (reference frame fixed to the rotor). In this sense, the Wigner function $W_\rho(\Theta, j)$ can be asymptotically considered as a distribution in a four-dimensional manifold.

3. Classical point of view

In spite of the simplicity of equation (14), it does not fit with the standard description of a classical rotor, since, according to the form of the Darboux coordinates in this representation, the quantization axis (which is always parallel to the total angular momentum) is tight to the axis z' in the non-inertial reference frame. This means that classically the rotor axis lies in the plane orthogonal to the z'-axis, so that the moment of inertia $I_{x'} = 0$ (the axis of the rotor is along x'), while $I_{y'} = I_{z'}$, so that only two angles are sufficient to specify the position of the rotor (in contrast to the symmetric top case, when three angles are required). Thus, the quantization axis is related to the total angular momentum and not to the axis of the rigid rotor (see figure 1). For an intuitive description of the orientation of the rotor axis, it is advantageous to change the quantization axis from the z- to the x-axis, and the polar angle θ corresponds then to the angle between the z- and rotor axes (see figure 2). This change of reference axis allows for an interpretation of the rotor motion consistent with the classical picture [26], where $I_{x'} = I_{y'}$ and $I_{z'} = 0$, and the position of the rotor is defined by the angles θ and ϕ, as is indicated in figure 2. In order to change the quantization axis from z to x, we therefore apply a $\pi/2$-rotation around the y-axis to the kernel (equation (4)), to obtain

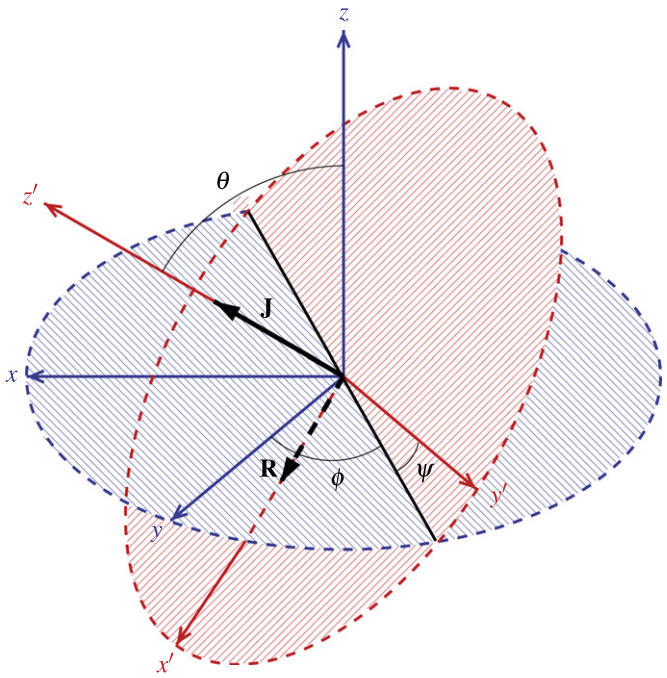

Figure 1. The position of the (non-inertial) (x', y', z') reference frame tight to the rotor with respect to the inertial (x, y, z) reference frame in terms of Euler angles (ϕ, θ, ψ). The rotor axis **R** is aligned along the axis x′ so that the moments of inertia are $I_{x'} = 0$ and $I_{y'} = I_{z'}$.

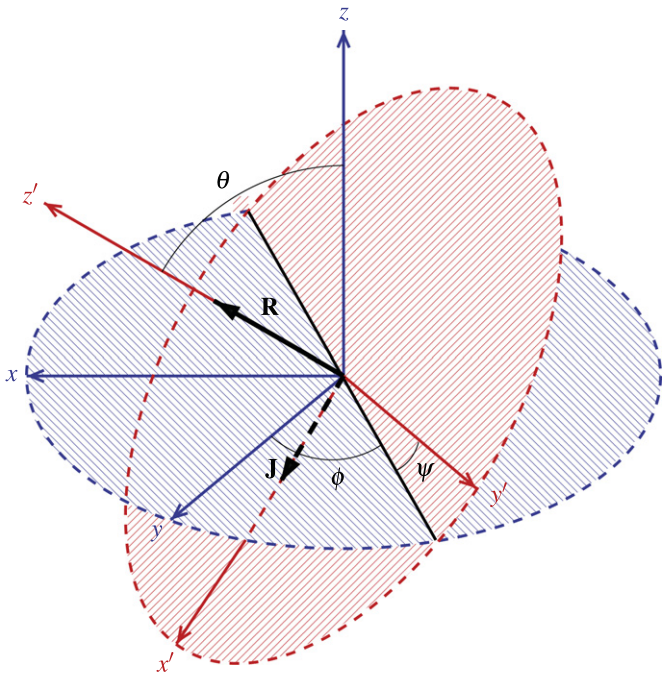

Figure 2. The position of the rotor after $\pi/2$ rotation around y' axis. The rotor is aligned along the z' axis so that $I_{z'} = 0$ and $I_{x'} = I_{y'}$. The total angular momentum **J** is directed along the x' axis.

$$\hat{\omega}_j^{\,y}(0) = \mathrm{e}^{-\mathrm{i}\pi/2\hat{J}_y}\,\hat{\omega}_j(0)\,\mathrm{e}^{\mathrm{i}\pi/2\hat{J}_y} = \sum_{K=0}^{j}\sum_{q,q'=-K}^{K}\sqrt{\frac{2K+1}{j+1}}\,\mathrm{d}^{K}_{qq'}(\pi/2)\,T^{\frac{j+q'}{2}\frac{j-q'}{2}}_{Kq}, \tag{15}$$

where the Wigner d matrix is given by $\mathrm{d}^{j}_{mm'}(\theta) = \langle j, m|\ \mathrm{e}^{-\mathrm{i}\theta\hat{J}_y}\ |j, m'\rangle$. Then, the quantization axis coincides with the body symmetry axis, and the kernel acquires the form

$$\hat{\omega}_j^{\gamma}(\Theta) = \hat{D}(\Theta)\hat{\omega}_j^{\gamma}(0)\hat{D}^{\dagger}(\Theta) = \sum_{K=0}^{j}\sum_{q,q'=-K}^{K}\sqrt{\frac{2K+1}{j+1}}D_{qq'}^{K}\left(\Theta'\right)T_{Kq}^{2\,\frac{j+q'}{2}\,\frac{j-q'}{2}}, \tag{16}$$

where the Wigner D matrix is defined as $D_{mm'}^{j}(\Theta) = \langle j,\ m|\ \hat{D}(\Theta)|j,\ m'\rangle$, and Θ' are the rotated angles determined by

$$\begin{aligned}\sin\theta'\,\sin\left(\phi'-\phi\right) &= \sin\psi,\\ \sin\theta'\,\sin\psi' &= \sin\psi\,\sin\theta,\\ \cos\theta' &= -\sin\theta\,\cos\psi.\end{aligned} \tag{17}$$

In other words, the transformation equation (15) leads to the standard classical picture: the rotor axis is along the z' axis, while its angular momentum is in the x'-y' plane. The Darboux coordinates in new coordinates can be obtained directly from the conjugate pairs $((j+1)\cos\theta,\ \phi)$ and $(j,\ \psi)$ by the change of variables equation (17), representing a canonical transformation. Then, the Darboux coordinates in this representation become $(p_\theta,\ \theta)$ and $(p_\phi,\ \phi)$, where the conjugate momenta to coordinates θ and ϕ are [27]

$$p_\theta = (j+1)\sin\psi, \tag{18}$$

$$p_\phi = (j+1)\sin\theta\,\cos\psi. \tag{19}$$

On the other hand, as is seen in figure 2, the conjugate momentum to the coordinate θ is just the projection of the angular momentum $\mathbf{J}$ to the line of nodes, and the conjugate momentum to ϕ is the (negative) projection of $\mathbf{J}$ to the z-axis; since the rotor is aligned along the z'-axis, which is orthogonal to $\mathbf{J}$, no conjugate momentum to ψ exists.

4. Rigid rotor in an external field

Let us consider the following Hamiltonian governing the evolution of a quantum rigid rotor in an external field directed along the z-axis,

$$H = B\hat{J}^2 - g\hat{n}_z^2, \tag{20}$$

where $B = (2I)^{-1}$ with I being the moment of inertia ($\hbar = 1$) and $g > 0$. This is the model for an anisotropically polarizable molecule interacting with off-resonant light of intensity I_0, linearly polarized in the z-direction, where $g = \frac{1}{4}(\alpha_\parallel - \alpha_\perp)I_0$, with $\alpha_\parallel > \alpha_\perp$ being the molecular polarizabilities parallel and perpendicular to the molecular symmetry axis [28–41]. The external field produces a dynamical alignment of the molecular axis along the direction of the external field (z-axis).

The molecular alignment has been shown to enhance bimolecular and photochemical reactions [42] and high-harmonic generation [43] and to be crucial for attosecond physics [44], the ionization rate of the molecule [45–49], the molecular dipole force [50, 51], and laser filamentation [52]. The quantum-theoretical description of this dynamics leads to a set of coupled equations of motion for the state amplitudes whose size depends on the number of rotational levels that are taken into account, so that the numerical simulation is the only possible treatment even in the case of low rotational excitations. Here we apply our semiclassical treatment and compare it later (see section 5), to the solution of the exact quantum-mechanical problem.

The operator $\hat{n}_z$ (equation (11)), acts on the spherical harmonics as

$$\hat{n}_z\,Y_{lm}(\theta,\ \phi) = \cos\theta Y_{lm}(\theta,\ \phi) \tag{21}$$

where θ is the angle between the molecular axis and the applied electric field (z-axis). A substantial degree of alignment of the molecular axis along the z-direction is obtained for sufficiently strong intensities, $g \gg B$, and a commonly used measure for this alignment is given by the expectation value $\langle \hat{n}_z^2 \rangle$.

We suppose that initially the rotor is highly excited, and its angular momentum is aligned in a certain direction $(\vartheta_0,\ \varphi_0)$. This corresponds to the initial SU(2) coherent state

$$\left|l_0,\ \vartheta_0,\ \varphi_0\right\rangle = \sum_{m=-l_0}^{l_0}\sqrt{\frac{\left(2l_0\right)!}{\left(l_0-m\right)!\left(l_0+m\right)!}}\,\mathrm{e}^{-\mathrm{i}m\varphi_0}\sin^{l_0-m}\frac{\vartheta_0}{2}\cos^{l_0+m}\frac{\vartheta_0}{2}\left|l_0,\ m\right\rangle, \tag{22}$$

in a subspace with a large value of the orbital (l_0 is an integer) quantum number $l_0 \gg 1$. Such types of molecular states are generated by the use of an optical centrifuge, which drives the rotational energy to very high values by applying a chirped laser pulse to the anisotropically polarizable non-polar molecule [53–56]. In this semiclassical limit we can apply equation (14) in order to determine the rotor's dynamics.

Without loss of generality we may choose $\varphi_0 = 0$. Then the j-symbol of the density operator, the j-Wigner function $W_\rho(\Theta,\ j) = Tr(\hat{\omega}_j^{\gamma}(\Theta)\rho)$, corresponding to the initial coherent state $|l_0,\ \vartheta_0,\ \varphi_0 = 0\rangle$, which is localized

in a subspace of dimension $2l_0 + 1$, has the form

$$W_\rho(\Theta, j\,|t=0) = \delta_{j,2l_0}\sum_{K=0}^{2l_0}\frac{2K+1}{2l_0+1}\mathrm{e}^{-K(K+1)/2\left(2l_0+1\right)}P_K\left(\cos\theta''\right), \tag{23}$$

where $P_K(z)$ is the Legendre polynomial, and its argument is determined by

$$\cos\theta'' = \cos\theta'\cos\vartheta_0 + \sin\theta'\sin\vartheta_0\cos\phi', \tag{24}$$

$$\cos\theta' = -\sin\theta\cos\psi, \quad \cot\left(\phi' - \phi\right) = \cos\theta\cot\psi. \tag{25}$$

Taking into account equation (10) and the approximate expression for the symbol of $\hat{n}_z^2$

$$W_{n_z}^j(\Theta) = Tr(\hat{\omega}_j^y(\Theta)n_z^2) \approx \cos^2\theta\sum_{n=0,1,..}\delta_{j,2n} + O\left(j^{-2}\right), \tag{26}$$

we arrive at the symbol of the Hamiltonian

$$W_H^j(\Theta) = B\frac{j}{2}\left(\frac{j}{2}+1\right) - g\cos^2\theta = H_{cl}. \tag{27}$$

Using the dimensionless time $\tau = Bt$ together with the dimensionless interaction strength $\kappa = g/B$, the truncated evolution equation (14) in new coordinates (equations (18) and (19)) for $W_\rho(\Theta, j)$ takes then the form

$$\begin{aligned}\partial_\tau W_\rho = (j+1)&\left(\frac{\cos\psi}{\sin\theta}\partial_\phi W_\rho + \sin\psi\partial_\theta W_\rho + \frac{\cos\theta\cos\psi}{\sin\theta}\partial_\psi W_\rho\right)\\ &- 4\kappa\cos\theta\sin\theta\sin\psi\partial_j W_\rho - 4\kappa\frac{\cos\theta\sin\theta\cos\psi}{j+1}\partial_\psi W_\rho.\end{aligned} \tag{28}$$

The general solution of the above equation is

$$\begin{aligned}W_\rho(\Theta, j\,|\tau) = \int_0^\infty \mathrm{d}j_0\frac{j_0+1}{8\pi^2}\int \mathrm{d}\Theta_0\delta^{(3)}\left(\Theta - \Theta\left(\Theta_0, j_0\,|\tau\right)\right)\\ \times\,\delta\left(j - j\left(\Theta_0, j_0\,|\tau\right)\right)W_\rho\left(\Theta_0, j_0\,|\tau=0\right)\end{aligned} \tag{29}$$

where $\Theta(\Theta_0, j_0\,|\tau) = (\phi(\Theta_0, j_0\,|\tau), \theta(\Theta_0, j_0\,|\tau), \psi(\Theta_0, j_0\,|\tau))$, and $j(\Theta_0, j_0\,|\tau)$ are the classical trajectories defined by the following coupled set of first-order differential equations obtained from equation (28) by using the method of characteristics,

$$\frac{\mathrm{d}\theta}{\mathrm{d}\tau} = (j+1)\sin\psi, \tag{30}$$

$$\frac{\mathrm{d}\phi}{\mathrm{d}\tau} = \frac{(j+1)\cos\psi}{\sin\theta}, \tag{31}$$

$$\frac{\mathrm{d}\psi}{\mathrm{d}\tau} = \frac{(j+1)\cos\theta\cos\psi}{\sin\theta} - 4\kappa\frac{\cos\theta\sin\theta\cos\psi}{j+1}, \tag{32}$$

$$\frac{\mathrm{d}j}{\mathrm{d}\tau} = -4\kappa\cos\theta\sin\theta\sin\psi. \tag{33}$$

The above characteristic equations describe the classical dynamics of a rotor governed by the classical Hamiltonian H_{cl} (equation (27)). The initial values $\Theta_0 = (\phi_0, \theta_0, \psi_0)$ and j_0 are distributed according to the phase-space distribution (equation (23)).

It is easy to see that the above system admits two integrals of motion: p_ϕ and the total energy, as is expected.

According to equation (9) the time-dependent alignment is computed as

$$\left\langle\hat{n}_z^2(\tau)\right\rangle = \int_0^\infty \mathrm{d}j_0\frac{j_0+1}{8\pi^2}\int \mathrm{d}\Theta_0\frac{j\left(\Theta_0, j_0\,|\tau\right)+1}{8\pi^2}\cos^2\theta_0 W_\rho\left(\Theta_0, j_0\,|\tau=0\right), \tag{34}$$

where the integration is extended over the points of the initial distribution (equation (23)).

In order to relate the Hamiltonian picture of the rotor motion, (equations (30)–(33)), to the standard Euler description, we compute the angular velocities in the non-inertial reference frame, considering the rotor being aligned along the z'-axis in the non-inertial reference frame,

$$\Omega_{x'} = -\dot{\phi}\sin\theta\cos\psi + \dot{\theta}\sin\psi, \tag{35}$$

$$\Omega_{y'} = \dot{\phi}\sin\theta\sin\psi + \dot{\theta}\cos\psi, \tag{36}$$

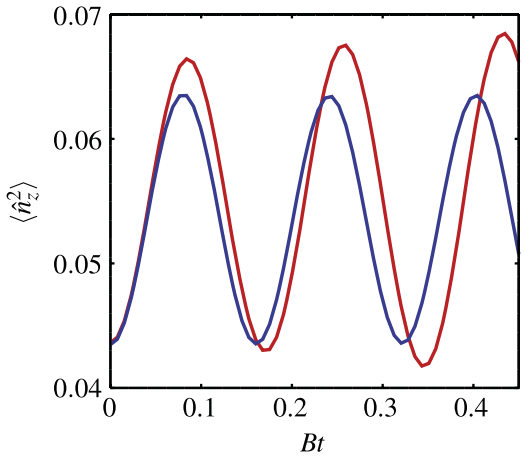

Figure 3. Alignment $\langle \hat{n}_z^2 \rangle$ of a rigid-rotor molecule with initial angular-momentum coherent state $|l_0 = 10,\ \vartheta_0 = 0\rangle$, as a function of the dimensionless time Bt for the dimensionless interaction strength $\kappa = 50$. The semiclassical solution (red) is compared with the exact solution of the Schrödinger equation (blue).

$$\Omega_{z'} = \dot{\phi}\cos\theta + \dot{\psi}. \tag{37}$$

Then, the angular momenta (in our case the moments of inertia $I_{x'} = I_{y'} = I$, $I_{z'} = 0$) $J_{x'} = I\Omega_{x'}$ and $J_{y'} = I\Omega_{y'}$ lead to the total momentum

$$J^2 = J_{x'}^2 + J_{y'}^2 = I^2\left(\dot{\phi}^2\sin^2\theta + \dot{\theta}^2\right) = (j+1)^2/4, \tag{38}$$

where the last relation is obtained by using equation (30).

5. Numerical solution

To illustrate the above-developed method we may now apply it numerically to obtain the alignment dynamics of a rigid rotor-type molecule. The initial phase-space distribution is binned in the angles $\Theta = (\phi, \theta, \psi)$ on a $80 \times 40 \times 80$ grid, where from each centred grid point a trajectory is numerically calculated according to equations (30)–(33). To obtain the time-dependent phase-space distribution, the end points of these trajectories are weighted by the values of the binned initial phase-space distribution taken at the originating points. The time-dependent alignment is then obtained by sampling according to equation (34).

We choose two particular initial states, both being angular-momentum coherent states, $|l_0,\ \vartheta_0\rangle$ with $l_0 = 10$, but with different directions, $\vartheta_0 = 0$ and $\vartheta_0 = \pi/2$, of their mean angular momentum.

For the case when the initial orientation of the mean angular momentum is in the direction of the z-axis ($\vartheta_0 = 0$), the molecular axis is rotating (on average) in the x-y plane, and, therefore, the alignment parameter $\langle \hat{n}_z^2 \rangle$ is initially at its minimum value, deviating from zero only by the quantum fluctuations in the molecular axis direction of the initial coherent state. Later on, a maximum alignment at short times can be appreciated that is followed by an oscillation (see red curve in figure 3). To explain this dynamics we may consider the semiclassical effective potential, which the angle θ of the molecular axis is subjected to. As the initial coherent state coincides with the angular momentum eigenstate $|l_0,\ l_0\rangle$, it is clear that a strong centrifugal potential barriers appear at the poles, i.e., for molecular axis angles $\theta = 0$ and $\theta = \pi$ (see left part of figure 4). Due to these barriers, the molecular axis cannot completely align to the external field direction (i.e., the z-axis) but is reflected from the barrier at the poles and continues with an oscillatory dynamics that for larger κ is of the double-well type.

When compared with the exact solution of the corresponding Schrödinger equation, as shown by the blue curve in figure 3, we may observe an increasing deviation from the exact solution after the first maximum. Besides, the time interval for which the semiclassical approximation remains valid decreases with decreasing angular momentum. For instance, numerical simulations using $l_0 = 4$ show that deviation from the exact result in the vicinity of the first minimum is of the order of 10%, while for $l_0 = 10$ this error is roughly 5%.

It should be stressed here that in the framework of a one-dimensional approach, the standard semiclassical approximation fails to describe even the principal characteristics of a quantum system when the total energy is close to the bottom of the effective semiclassical potential energy. A relatively good agreement between quantum and semiclassical calculations is explained by the kind of the perturbation theory we have employed (equation (14)), where the real semiclassical parameter is the intensity of the rotational excitations rather than the gap between total and potential energies.

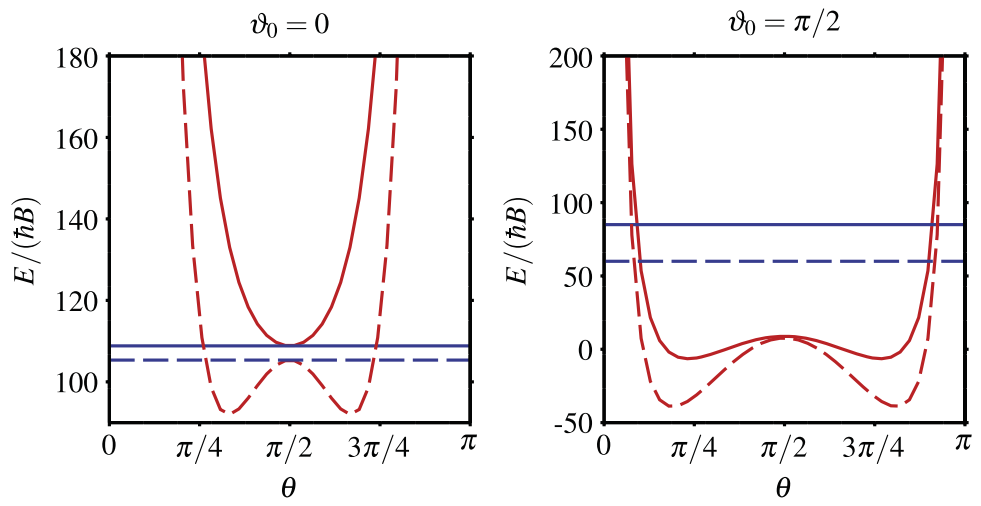

Figure 4. Semiclassical effective potential (red) and energy (blue) for the alignment angle θ. In the case of the initial coherent state $|l_0 = 10,\ \vartheta_0 = 0\rangle$ (left figure), the potential reads $V_0(\theta) = l_0(l_0 + 1)/\sin^2\theta - \kappa\cos^2\theta$, which is shown for $\kappa = 50$ (solid line) and $\kappa = 200$ (dashed line). For the initial coherent state $|l_0 = 10,\ \vartheta_0 = \pi/2\rangle$ (right figure) the potential reads $V_{\pi/2}(\theta) = l_0/\sin^2\theta - \kappa\cos^2\theta$, which is shown for $\kappa = 50$ (solid line) and $\kappa = 100$ (dashed line).

As was mentioned in section 2, the Wigner function $W_\rho^j(\Theta)$ can be asymptotically considered as a distribution in a four-dimensional phase-space, $W_\rho^j(\Theta) \approx W_\rho(\Theta, j)$ or $W_\rho^j(\Theta) \approx W_\rho(p_\theta, p_\phi, \theta, \phi)$, in terms of the angles (θ, ϕ) and the corresponding conjugate momenta. It is illustrative to observe the rotor dynamics in the reduced phase-space (p_θ, θ), where the marginal distribution function is obtained by the integration over (p_ϕ, ϕ),

$$W_\rho(p_\theta, \theta) = \int_{-\infty}^{\infty} \mathrm{d}p_\phi \int_0^{2\pi} \mathrm{d}\phi\, W_\rho(p_\theta, p_\phi, \theta, \phi). \tag{39}$$

In figure 5 this dynamics is shown for times corresponding to the initial state (upper left), the first maximum (upper right), the first minimum (lower left), and the second maximum (lower right) in the alignment shown in figure 3. Of course, as the distribution is shown on a 'reduced' phase space, the state does not look well localized in the sense of a semiclassical state. In fact, substantial interference fringes can be observed throughout the time evolution. However, in the full four-dimensional phase-space, the state is well localized for a sufficiently long time.

Rather different is the situation for an initial coherent state with the orientation of the mean angular momentum within the x-y plane; i.e., for $\vartheta_0 = \pi/2$. In this initial state the molecular axis is rotating, say, around the x-axis, and thus the centrifugal barriers at $\theta = 0$ and π are now less strong, allowing for the external field to contribute to the semiclassical effective potential in the form of a double well (see right part of figure 4). Thus there is no substantial centrifugal effect that may limit the alignment of the molecular axis along the direction of the external field (z-axis). Thus an oscillation is observed due to the initial rotation of the molecule that periodically maximizes the alignment (see figure 6). Over time the oscillation of the semiclassical solution (red curve) is damped, whereas the exact solution keeps oscillating (blue curve). However, in this case, as the energy is much higher than the bottom of the potential (see figure 4), the semiclassical approach is well justified, as can be seen from the much lower deviation from the exact solution as compared to the case $\vartheta_0 = 0$ (see figures 3 and 6).

The evolution of the reduced Wigner function $W(p_\theta, \theta)$ is in figure 7 for the interaction strength $\kappa = 100$ at times corresponding to the initial state (upper left), the first maximum (upper right), the first minimum (lower left), and the second maximum (lower right) in the alignment shown in figure 6. In can be seen that the range of angles is now substantially larger than in the case $\vartheta_0 = 0$, as is to be expected due to the weaker centrifugal barrier.

6. Summary and conclusions

In summary we have shown how a phase-space representation of a rigid-rotor motion can be developed that satisfies both SO(3) group covariance and also includes information about all correlations between invariant subspaces. It is thus a complete description that also allows a physical interpretation of the resulting Wigner function in terms of standard Hamiltonian mechanics, including its projection on the reduced phase space.

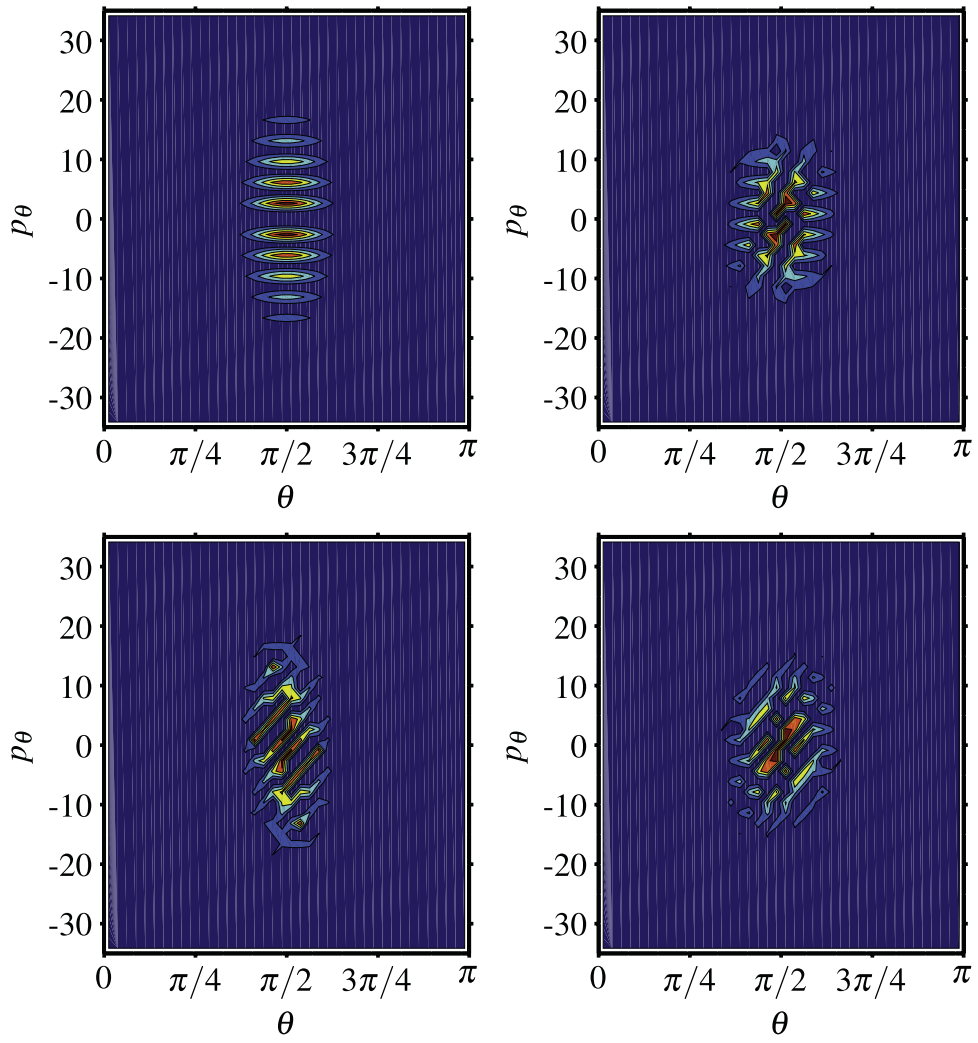

Figure 5. Evolution of the reduced Wigner function $W(\theta, p_\theta)$ for the initial coherent state $|l_0 = 10, \vartheta_0 = 0\rangle$ for $\kappa = 50$ and for the dimensionless times Bt: 0.00 (upper left), 0.08 (upper right), 0.16 (lower left), and 0.25 (lower right). From blue to red, the value of the Wigner function increases from zero to positive values (same colour scale for all plots).

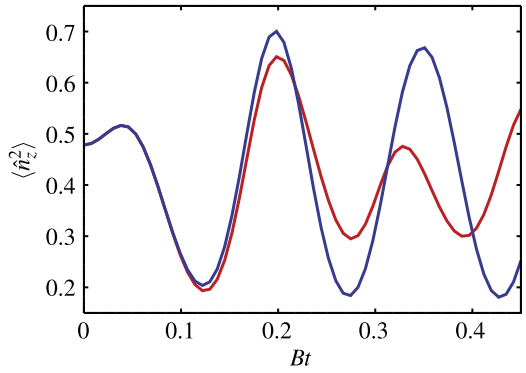

Figure 6. Alignment $\langle \hat{n}_z^2 \rangle$ of a rigid-rotator molecule with initial angular-momentum coherent state $|l_0, \vartheta_0 = \pi/2\rangle$ with $l_0 = 10$ as a function of the dimensionless time Bt and for the dimensionless interaction strength $\kappa = 100$. The semiclassical solution (red) is compared with the exact solution of the Schrödinger equation (blue).

Moreover, a natural semiclassical parameter exists in this representation, which is the inverse number of rotational excitations j. For large j a semiclassical approximation can be devised that allows us to describe the quantum dynamics by the classical trajectories that originate at an initial quantum phase-space distribution. These phase-space trajectories have been shown to be perfectly compatible with the classical Euler dynamics of a

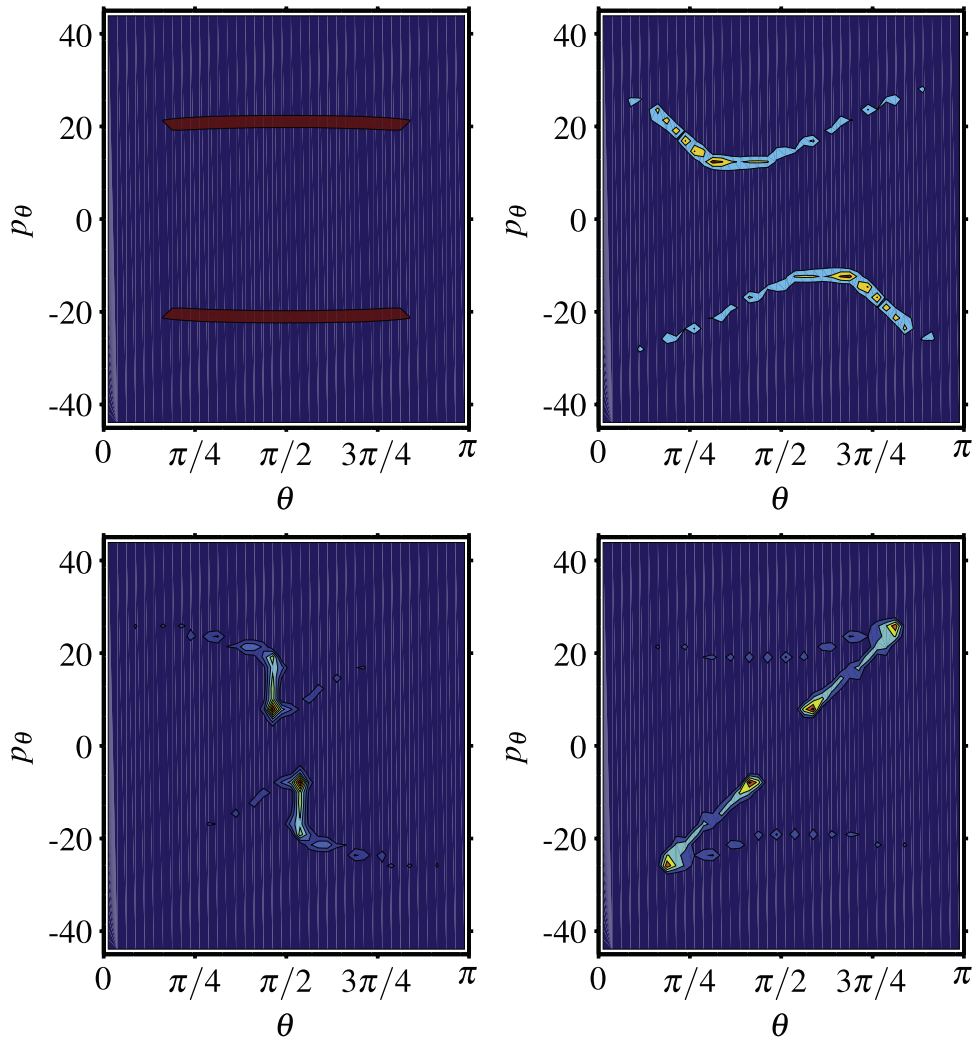

Figure 7. Evolution of the reduced Wigner function $W(\theta, p_\theta)$ for the initial coherent state $|l_0, \vartheta_0 = \pi/2\rangle$ for $l_0 = 10$ and for the dimensionless times Bt: 0.00 (upper left), 0.05 (upper right), 0.11 (lower left), and 0.16 (lower right). From blue to red, the value of the Wigner function increases from zero to positive values (same colour scale for all plots).

rigid rotor and thus can be interpreted in the standard classical way [26]. Thus, the semiclassical dynamics in our SO(3) covariant approach is described in a standard form: each point of the initial distribution in a four-dimensional manifold evolves along a classical trajectory, which results in a deformation of the initial distribution. Such deformation describes quite well the system's dynamic with a variable number of rotational excitations, even for a moderate times.

It is important to stress that the type of map used as an interface between the quantum and classical worlds is of great importance, since it fixes the structure of the phase-space manifold. The requirement of covariance of the mapping under a given dynamical group leads to a description of the quantum evolution in terms of trajectories in manifolds with corresponding transformation properties. As a consequence, the phase-space dynamics is characterized by semiclassical parameters related both to the symmetry of the interaction Hamiltonian and the symmetry of the mapping. For instance, the physical semiclassical parameter characteristic for mappings covariant under the Heisenberg–Weyl group H(1) is the inverse number of excitations in the corresponding one-dimensional system (the average number of photons in a field mode, the total energy of a massive particle moving in a one-dimensional potential, etc). In the case of spin systems, the role of such semiclassical parameters plays the inverse spin length, or, in algebraic terms, the dimension of the representation of the SU(2) group.

In this sense the precision of the quantum evolution description of a rigid rotor by using the present SO(3) covariant mapping, where the semiclassical parameter is the inverse number of rotational excitations, in principle should be better than in the previously developed $E(2) \times E(2) \times E(2)$ covariant approach [15], where the physical semiclassical parameters, which are the inverse angular momenta corresponding to each Euler angle [57], are associated with independent mapping kernels (while the formal expansion parameter is the

Planck constant). In other words, although the equation of motion obtained in [15], projected from the six-dimensional phase-space of a top to the four-dimensional phase-space of a rigid rotor, coincides (in appropriate variables) with the evolution equation (14), the accuracy of the semiclassical description is heavily determined by the type of employed mapping.

We have applied our theory to the case of alignment of molecules by strong external fields and have shown that by rather simple numerical procedures, the quantum alignment dynamics of highly rotationally excited molecules can be quite well described. This coincides with the numerical solution of the exact problem within a sufficiently large time period in order to describe the maximally possible alignment. In conclusion, this semiclassical treatment may serve as an alternative and numerically more feasible method, as compared to direct integration of the Schrödinger wave equation.

Acknowledgments

This research was supported by the International Scientific Cooperation Project CONACYT-CONICYT 2011-557 and CONACYT 174713.

References

[1] Hillery M, O'Connel R F, Scully M O and Wigner E P 1984 *Phys. Rep.* **106** 121
[2] Lee H W 1995 *Phys. Rep.* **259** 147
Zachos C K, Fairle D B and Curtright T L 2005 *Quantum Mechanics in Phase-Space* (Singapore: World Scientific)
[3] Schleich W P 2001 *Quantum Optics in Phase-Space* (New York: Wiley)
[4] Glauber R J 1963 *Phys. Rev. Lett.* **10** 84
[5] Sudarshan E C G 1963 *Phys. Rev. Lett.* **10** 177
[6] Cahill K E and Glauber R J 1969 *Phys. Rev.* A **177** 1857
[7] Agarwal G S and Wolf E 1968 *Phys. Rev. Lett.* **21** 180
[8] Berezin P A 1975 *Comm. Math. Phys.* **40** 153
[9] Cohen L J 1966 *J. Math. Phys.* **7** 781
Cohen L J 1976 *J. Math. Phys.* **17** 1863
[10] Brif C and Mann A 1999 *Phys. Rev.* A **59** 971
[11] Mukunda N, Marmo G, Zampini A, Chaturvedi S and Simon R 2005 *J. Math. Phys.* **46** 012106
[12] Stratonovich R L 1956 *Sov. Phys. JETP* **31** 1012
[13] Agarwal G S 1981 *Phys. Rev.* A **24** 2889
[14] Várilly J C and Gracia-Bondía J M 1989 *Ann. Phys.* **190** 107
[15] Fischer T, Gneiting C and Hornberger K 2013 *New J. Phys.* **15** 063004
[16] Gneiting C, Fischer T and Hornberger K 2013 *Phys. Rev.* A **88** 062117
[17] Moyal J E 1949 *Proc. Cambridge Phil. Soc* **45** 99
[18] Ballentine L E, Yang Y and Zibin J P 1994 *Phys. Rev.* A **50** 2854
[19] Kinsler P and Drummond P D 1997 *Phys. Rev.* A **44** 7848
[20] Drobný G, Bandilla A and Jex I 1997 *Phys. Rev.* A **55** 78
[21] Heller E J, Reimers J R and Drolshagen J 1987 *Phys. Rev.* A **190** 2613
[22] Klimov A B 2002 *J. Math. Phys* **43** 2202
[23] Klimov A B and Espinoza P 2005 *J. Opt. B: Quantum Semiclass. Opt.* **7** 183
[24] Polkovnikov A 2010 *Ann. Phys.* **325** 1790
[25] Klimov A B and Romero J L 2008 *J. Phys.* A **41** 055303
[26] Landau L D and Lifshitz E M 1960 *Mechanics* (Oxford: Pergamon Press)
[27] Dubrovin B A, Krichever I M and Novikov S P 2001 *Encyclopaedia of Mathematical Sciences, Integrable Systems I* **4** 177–332
[28] Friedrich B and Herschbach D R 1992 *Z. Phys.* D **24** 25
[29] Slenczka A, Friedrich B and Herschbach D R 1994 *Phys. Rev. Lett.* **72** 1806
[30] Rost J M, Griffin J C, Friedrich B and Herschbach D R 1992 *Phys. Rev. Lett.* **68** 1299
[31] Loesch H J and Möller J 1993 *J. Phys. Chem.* **97** 2158
[32] Normand D, Lompre L A and Cornaggia C 1992 *J. Phys.* B **25** L497
[33] Friedrich B and Herschbach D R 1995 *Phys. Rev. Lett.* **74** 4623
[34] Takekoshi T, Patterson B M and Knize R J 1998 *Phys. Rev. Lett.* **81** 5105
[35] Seideman T 1995 *J. Chem. Phys.* **103** 7887
[36] Seideman T 2001 *J. Chem. Phys.* **115** 5965
[37] Dooley P W, Litvinyuk I V, Lee K F, Rayner D M, Spanner M, Villeneuve D M and Corkum P B 2003 *Phys. Rev.* A **68** 023406
[38] Stapelfeldt H and Seideman T 2003 *Phys. Mod. Rev.* **75** 543
[39] Seideman T and Hamilton E 2006 *Adv. At. Mol. Opt. Phys.* **52** 289
[40] Adelswärd A, Wallentowitz S and Vogel W 2003 *Phys. Rev.* A **67** 063805
Adelswärd A, Wallentowitz S and Vogel W 2003 *Phys. Rev.* A **68** 049901
[41] Adelswärd A and Wallentowitz S 2004 *J. Opt.* B **6** S147
[42] Stapelfeldt H 2004 *Phys. Scr.* T **110** 132
[43] Itatani J, Zeidler D, Levesque J, Spanner M, Villeneuve D M and Corkum P B 2005 *Phys. Rev. Lett.* **94** 123902
[44] Haessler S *et al* 2010 *Nat. Phys.* **6** 200
[45] Litvinyuk I V, Lee K F, Dooley P W, Rayner D M, Villeneuve D M and Corkum P B 2003 *Phys. Rev. Lett.* **90** 233003
[46] Zhao Z X, Tong X M and Lin C D 2003 *Phys. Rev.* A **67** 043404

[47] Smeenk C T L, Arissian L, Sokolov A V, Spanner M, Lee K F, Staudte A, Villeneuve D M and Corkum P B 2014 *Phys. Rev. Lett.* **112** 253001
[48] Lee S K, Lin Y F, Yan L and Li W 2012 *J. Phys. Chem.* A **116** 1950
[49] Hansen J L, Holmegaard L, Nielsen J H, Stapelfeldt H, Dimitrovski D and Madsen L B 2012 *J. Phys.* B **45** 015101
[50] Purcell S M and Barker P F 2010 *Phys. Rev.* A **82** 033433
[51] Gershnabel E and Averbukh I S 2011 *J. Chem. Phys.* **135** 084307
[52] Wu J, Cai H, Peng Y, Tong Y, Couairon A and Zeng H 2009 *Laser Phys.* **19** 1759
[53] Karczmarek J, Wright J, Corkum P B and Ivanov M 1999 *Phys. Rev. Lett.* **82** 3420
[54] Villeneuve D M, Aseyev S A, Dietrich P, Spanner M, Ivanov M Y and Corkum P B 2000 *Phys. Rev. Lett.* **85** 542
[55] Spanner M and Ivanov M Y 2001 *J. Chem. Phys.* **114** 3456
[56] Spanner M, Davitt K M and Ivanov M Y 2001 *J. Chem. Phys.* **115** 8403
[57] Rigas I, Sánchez-Soto L L, Klimov A B, Rehacek J and Hradil Z 2011 *Ann. Phys.* **326** 426